

Determination of the parameters of semiconducting CdF₂:In with Schottky barriers from radio-frequency measurements

A. I. Ritus*, A. V. Pronin, and A. A. Volkov

Institute of General Physics, Russian Academy of Sciences, 119991 Moscow, Russia

P. Lunkenheimer and A. Loidl

Experimentalphysik V, EKM, Universität Augsburg, 86135 Augsburg, Germany

A. S. Shcheulin and A. I. Ryskin

S. I. Vavilov State Optical Institute, 195034 St. Petersburg, Russia

(Dated: October 26, 2018)

Physical properties of semiconducting CdF₂ crystals doped with In are determined from measurements of the radio-frequency response of a sample with Schottky barriers at frequencies 10 – 10⁶ Hz. The *dc* conductivity, the activation energy of the amphoteric impurity, and the total concentration of the active In ions in CdF₂ are found through an equivalent-circuit analysis of the frequency dependencies of the sample complex impedance at temperatures from 20 K to 300 K. Kinetic coefficients determining the thermally induced transitions between the deep and the shallow states of the In impurity and the barrier height between these states are obtained from the time-dependent radio-frequency response after illumination of the material. The results on the low-frequency conductivity in CdF₂:In are compared with submillimeter (10¹¹ – 10¹² Hz) measurements and with room-temperature infrared measurements of undoped CdF₂. The low-frequency impedance measurements of semiconductor samples with Schottky barriers are shown to be a good tool for investigation of the physical properties of semiconductors.

PACS numbers: 72.20.-i, 77.22.-d, 78.20.Ci

INTRODUCTION

CdF₂ belongs to a large family of fluorides crystallizing in the cubic fluorite structure *O5h (Fm3m)*, with parameters typical for this family: it is an ionic dielectric with a wide band gap and only one dipole-active lattice mode centered near $6 \cdot 10^{12}$ Hz [1]. The latter provides an almost frequency and temperature independent lower frequency (static) dielectric constant $\varepsilon \cong 8$ [1, 2].

If CdF₂ crystals doped with In are heated up in a reducing atmosphere of hydrogen or alkali metal vapors in a so-called additive coloration process, when a part of the interstitial F¹⁻ ions leaves the crystal, and afterwards are cooled down to a quite low temperature, half of the In ions reveal a completely ionized state, In³⁺, without any valence electron, and the other half exhibits an In¹⁺ state, with two valence electrons [3, 4]. Thus the non-local neutrality of the crystals is satisfied, and almost full self-compensation of the donor impurities is realized. Since, due to the Coulomb interaction, a localization of two electrons at one orbital is energetically not profitable, a compensating local lattice distortion appears around the In¹⁺ ions, the ions being moved along a 4th order axis into a neighboring cell of eight F¹⁻ ions not occupied by a Cd ion [5]. Consequently, a transition of the In ion from In³⁺ state into the In¹⁺ state requires a local

lattice distortion. In other words, there is a significant potential barrier between the In¹⁺ and In³⁺ states. Thus, In¹⁺ impurities in CdF₂ form a deep level, which is similar to the *DX*-centers in typical semiconductors [6, 7]. A fraction of electrons is captured by In³⁺ ions, forming a hydrogen state (In³⁺ + *e_{hydr}*), a shallow donor level, being the basic reason that the CdF₂:In reveals semiconducting properties. The relative concentrations of the shallow In³⁺ + *e_{hydr}* and the deep In¹⁺ centers depend on the temperature. Fig. 1 shows an energy level diagram for the deep, *E_{deep}*, and the shallow, *E_{sh}*, states of the bistable In centers in CdF₂ as function of the configuration coordinate *Q* (position of the In impurity relative to the surrounding ions). For a transition from one state to another the electron has to overcome an additional capture barrier, *E_{cap}*, and consequently the upper state is metastable. The energy of the states measured from the bottom of the conducting band are *E_{deep}* = 0.25 eV [5] and *E_{sh}* \cong 0.1 eV [8]. The electrons of the *DX*-centers can be transferred to the shallow state either by light irradiation or by temperature. The changing of the *DX*-center state leads to a change of polarizability and, consequently, to a local change of the refractive index. This fact allows to use the metastable shallow states to write reversible phase holograms. The efficient writing of such holograms in the semiconducting CdF₂ doped with In or Ga has been demonstrated in [9] and [10]. The interest in these materials is caused mainly by their holographic application.

Traditionally, investigations of the semiconducting

*Electronic address: ritus@ran.gpi.ru

transport properties of doped CdF_2 were carried out using ohmic contacts. The technique to produce such contacts is quite complicated and often is a kind of art. In this paper we report on the radio-frequency investigations of $\text{CdF}_2:\text{In}$ which were carried out without a use of ohmic contacts. We have determined characteristic features of $\text{CdF}_2:\text{In}$, as the temperature dependencies of the dc conductivity and of the ion concentration on the donor level, the activation energy of impurities, E_a , the total concentration of the active In ions, N , the barrier height, E_{cap} , and the values of the kinetic coefficients which determine the speed of the thermally induced transfers between the deep and the shallow states of the In ions in the CdF_2 matrix. All these parameters have been defined from low frequency ($10 - 10^6$ Hz) measurements of the complex impedance of thin plane-parallel $\text{CdF}_2:\text{In}$ samples with metallic electrodes which were either sputtered on their surfaces or just brought into contact with the surfaces. This method is the basis of our previous study [11].

SAMPLES AND EXPERIMENT

In most of the experiments we used a homogeneous transparent plane-parallel sample of CdF_2 with an InF_3 concentration in the raw material of 0.02 mole %. This concentration of the In impurities gives the sample a red-brownish color. The absorption coefficient α for light with a wavelength of $\lambda = 488$ nm has been measured to be of the order of 50 cm^{-1} at room temperature. Control experiments have been also performed for a pure CdF_2 sample without In doping. Both surfaces of the sample have been covered by gold electrodes made by plasma sputtering. The area of each electrode was 20 mm^2 and the electrode thickness was about 10 nm. The light transmittance through this electrode for $\lambda = 488$ nm has been estimated as high as 50 %. For the experiments, where we used electrodes isolated from the sample by mica, the same electrodes have been sputtered on two pieces of mica, 35μ thick each. For the experiments with Teflon isolating linings we used polished brass electrodes of 18.5 mm^2 . Finally, additional measurements were also performed for a sample with contacts formed by silver paint. In all cases lead wires were glued to the electrodes by a conducting glue.

The sample was placed on a copper cold finger of a helium flow cryostat *Helix CTI Cryogenic model 22*. The temperature of the finger was monitored and controlled by a *Lake Shore 330* temperature controller with an accuracy of 0.01 K.

In order to illuminate the samples a plane Plexiglas window was made in the vacuum shield of the cryostat. An argon laser beam with a power up to 14 mW at $\lambda = 488$ nm was widened by a lens to illuminate the complete sample surface. The laser intensity could be continuously

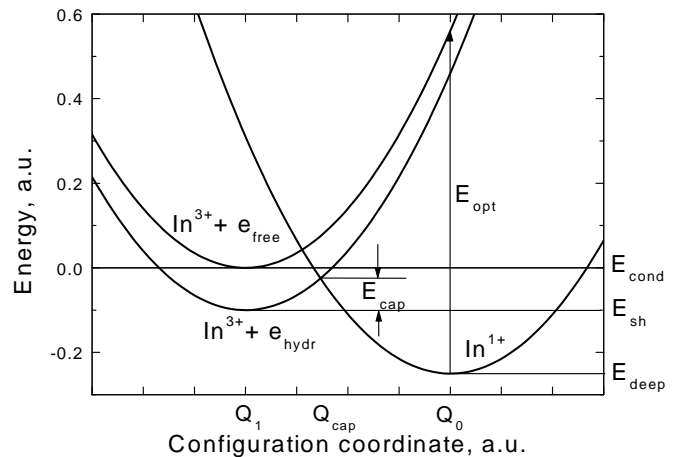


FIG. 1: Schematic diagram of the energy levels for the deep, E_{deep} , and the shallow, E_{sh} , states of the bistable In center in CdF_2 , as a function of the configuration coordinate Q of the In nucleus. E_{cap} - the barrier height between the shallow and the deep states, E_{cond} - the bottom of the conduction band, E_{opt} - the optical ionization energy of the deep state.

regulated by changing the gas discharge current in the laser tube, and by an external variable attenuator.

The lead wires from the electrodes were soldered to terminals of the cryostat. The terminals were connected with an LCR meter *HP4284A*. The analyzer *HP4284A* covers a frequency range from 20 to 10^6 Hz, an amplitude ac voltage V_s from 0 to 20 V and a bias voltage from -40 to 40 V. Usually $V_s = 0.1$ V and zero bias have been used. Results of the complex impedance of a sample with electrodes, Z , were obtained as an equivalent capacitance C_p and an equivalent conductance G_p (i.e. the complex conductance is $1/Z = G_p + i\omega C_p$, where ω is the angular frequency). Additional experiments have been carried out for frequencies extending to 320 MHz. In these experiments an *HP4191A* impedance analyzer with working range of 1 MHz - 1 GHz has been utilized. For the measurements the sample was placed at the end of a coaxial line, and a calibration procedure with three standard loads was required to eliminate the contributions of the line itself [12].

RESULTS AND DISCUSSION

Schottky barriers and a non-homogenous layered Maxwell-Wagner capacitor model

Typical results of our measurements of the frequency dependencies of C_p , and G_p/ν for the sample with gold electrodes are plotted in Fig. 2 ($\nu = \omega/2\pi$). These measurements were performed with the sample cooled in darkness. They clearly show the signature of a relaxation process for frequencies 20 Hz to 1 MHz, the relaxation frequency ν_p strongly depending on the temperature. When

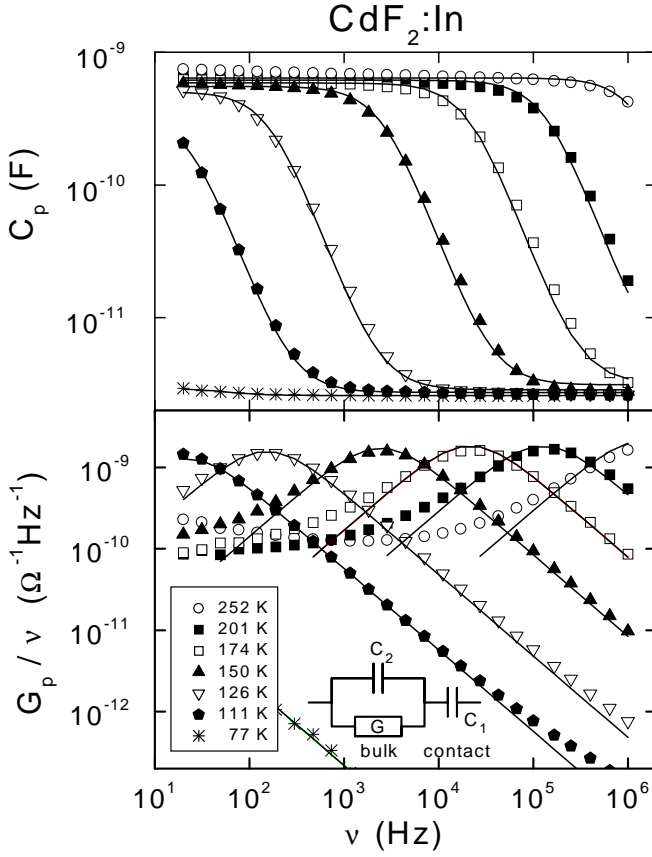


FIG. 2: Frequency dependencies of C_p (upper panel) and G_p/ν (bottom panel) for a sample with gold-sputtered electrodes at various temperatures. The points are experimental data, the solid lines are least square fits by formulas 3 and 4, deduced from the equivalent circuit indicated in the lower panel.

the temperature changes from 110 K to 200 K, ν_p rises by a factor of 10000.

Since in a cubic electronic semiconductor like CdF_2 : In it is very difficult to imagine a low frequency microscopic mechanism for this relaxation, we propose, that a macroscopic Maxwell-Wagner relaxation process accounts for this behavior. (This statement has been strongly supported by the experiments described below, where isolating layers between sample and electrodes have been used.) The Maxwell-Wagner relaxation is a quite common feature for a non-homogenous layered capacitor [13]. The layered structure results from the formation of Schottky barriers in the regions of semiconducting CdF_2 : In close to the metal electrodes [14]. If the electron work function φ_m in a metal is higher than in an electronic semiconductor, φ_s , the electron concentration in the contact region of the semiconductor is suppressed, and a depletion layer appears. Its thickness is equal to

$$d_c = \sqrt{2\varepsilon\varepsilon_0 V_c / en_d}, \quad (1)$$

where e is the electron charge, $V_c = (\varphi_m - \varphi_s)/e$ is the

contact potential difference, n_d is the donor concentration (total ionization of donors is supposed), and ε and ε_0 are the dielectric constants of the semiconductor and of the vacuum.

Thus, the sample with two electrodes may be considered as a structure of three condensers in series: two of them are formed by the depletion layers with small conductivity, and the third (the middle) one represents the bulk material with the real sample conductivity. If the material of both electrodes are the same and both sample surfaces had the same treatment, then two depletion-layer capacitors with capacity C' may be presented in the equivalent circuit scheme as one capacitor with capacitance $C_1 = C'/2$. The rest of the sample may be considered as a capacity C_2 with a parallel active conductivity G . Overall we arrive at the equivalent circuit indicated in Fig. 2. Neglecting the conductivity of the depletion layers, the impedance of this scheme is:

$$Z = \frac{1}{i\omega C_1} + \frac{1}{G + i\omega C_2}, \quad (2)$$

and the complex conductance is $1/Z = G_p + i\omega C_p$, where

$$G_p = \frac{C_1^2 \omega^2 G}{\omega^2 (C_1 + C_2)^2 + G^2}, \quad (3)$$

$$C_p = \frac{C_1 [G^2 + \omega^2 (C_1 C_2 + C_2^2)]}{\omega^2 (C_1 + C_2)^2 + G^2}. \quad (4)$$

An analysis of (3) and (4) shows that at $\omega \rightarrow 0$

$$C_p \rightarrow C_{p0} = C_1, \quad (5)$$

$$G_p \rightarrow G_{p0} = 0; \quad (6)$$

and at $\omega \rightarrow \infty$

$$C_p \rightarrow C_{p\infty} = C_1 C_2 / (C_1 + C_2), \quad (7)$$

$$G_p \rightarrow G_{p\infty} = G C_1^2 / (C_1 + C_2)^2. \quad (8)$$

If $C_1 \gg C_2$ (that usually holds for the Schottky barriers), then:

$$C_{p\infty} = C_2, \quad (9)$$

$$G_{p\infty} = G. \quad (10)$$

Thus, the high frequency limit represents the bulk material parameters, while the low frequency one depends strongly on the contact phenomena. In addition, $C_p(\omega_p) = (C_{p\infty} + C_{p0})/2$, where the relaxation frequency is:

$$\omega_p = 2\pi\nu_p = G / (C_1 + C_2). \quad (11)$$

TABLE I: Experimental values of ε and σ of the bulk material obtained from the radio-frequency measurements with three different kinds of linings at the electrodes: 1) Teflon linings, 2) mica linings, and 3) without any linings (marked as "Schottky barrier"). The values are presented for three temperatures. The experimental accuracy for ε is: 30 % for the Teflon linings, 20 % for the mica linings, and 10 % for the measurements without linings. The experimental accuracy for σ is: 30 % for the Teflon linings, 10 % for the mica linings, and 4 % for the measurements without linings.

T(K)	Teflon			Mica			Schottky barrier		
	109	124	148	109	124	148	110.5	125.3	149.4
ε	8.7	9.4	10.9	10.2	10.3	11.0	7.3	7.7	8.3
$\sigma(\Omega^{-1}\text{cm}^{-1})$	$1 \cdot 10^{-8}$	$1 \cdot 10^{-7}$	$1 \cdot 10^{-6}$	$1.4 \cdot 10^{-8}$	$1.3 \cdot 10^{-7}$	$2.2 \cdot 10^{-6}$	$1.3 \cdot 10^{-8}$	$1.2 \cdot 10^{-7}$	$2.2 \cdot 10^{-6}$

The frequency dependencies of C_p , and G_p/ν calculated from formulas 3 and 4 are shown in Fig. 2 as solid lines. The parameters C_1 , C_2 and G have been fitted with the least square method. As can be seen from Fig. 2, all the characteristic features of the experimental curves are well described by the formulas of the Maxwell-Wagner model [13]. For the higher temperatures, at low frequencies deviations of experimental data and fits show up in G_p/ν . They can be ascribed to a small, but non-zero conductivity of the depletion layers, which for very low frequencies would lead to a $1/\nu$ divergence. We note, that C_{p0} and $C_{p\infty}$ are almost temperature independent. Consequently, the strong temperature dependence of the relaxation frequency $\nu_p = G/2\pi(C_1 + C_2)$ is due to the temperature dependence of G . Using the temperature dependencies of the fitting parameters $C_2(T)$ and $G(T)$, we have calculated the real part of the dielectric permittivity $\varepsilon'(T) = C_2(T)d/(\varepsilon_0 S)$ and the conductivity $\sigma(T) = G(T)d/S$ of the bulk material (S is the electrode area, and d is the sample thickness).

Since the frequency dependencies of $C_p(\omega)$ and $G_p(\omega)$ (Eqns. 3 and 4) have the same shape as the frequency dependencies of ε' and $\sigma = \varepsilon''\varepsilon_0\omega$ for homogeneous dielectrics with Debye relaxation (here ε' and ε'' are real and imaginary parts of the dielectric permittivity), we have conducted two control experiments for the CdF₂: In sample with electrodes isolated from the sample by 55 μ thick Teflon ($\varepsilon_{Teflon} = 2$) and 35 μ thick mica ($\varepsilon_{mica} = 8$) layers. In these experiments no Schottky barriers are formed, and one can directly calculate the electrode capacitances $C' = 2C_1 \approx 2C_{p0}$ of the Maxwell-Wagner layered system. We have found, that the value of C_1 for Teflon is two orders of magnitude smaller and for mica it is one order of magnitude smaller than C_{p0} in the experiments with sputtered gold electrodes (2.5 pF and 20 pF, respectively), while C_2 remains at 3 - 4 pF. Accordingly, for a fixed temperature the values of C_{p0} decrease and the characteristic relaxation frequencies increase by 2 (1) orders of magnitude for Teflon (mica) linings. Such a behavior is expected in the case of a Maxwell-Wagner relaxation (see Eqn. 11), since the bulk conductance G does not depend on the type of the contacts. At the same time, in the case of the Debye relaxation, the characteristic frequency of which does not depend on the electrode

capacitances, one would obtain other, more complex, frequency dependencies of C_p and G_p due to a superposition of the Maxwell-Wagner relaxation and the Debye relaxation.

The evaluated values of ε' and σ of the bulk material are presented in Table I for three temperatures together with the values determined from the measurements with Schottky barriers. Table 1 documents, that the values of the dielectric constant and of the conductivity determined through the Maxwell-Wagner equivalent circuit analysis coincide with each other within experimental accuracy for all temperatures. This again proves the validity of the Maxwell-Wagner relaxation as a model for the treatment of our results.

According to the weak temperature dependence of $C_{p\infty}$, the capacity C_2 does not depend significantly on temperature: at temperatures between 70 K and 300 K $C_2 \approx 3$ pF, and consequently $\varepsilon \cong 8$ (at lowest T = 25 K, $\varepsilon \cong 7$). The same values of ε have been determined for an undoped sample. Contactless measurements made in the submillimeter frequency range give the same values for doped and pure CdF₂ as well [2].

Temperature and frequency dependencies of the conductivity

The temperature dependence of the conductivity obtained by fitting the experimental results $C_p(\omega)$, $G_p(\omega)$ with the Maxwell-Wagner model is shown in Fig. 3. For temperatures 100 K \div 250 K the temperature dependence of the conductivity can be well described by a thermally activated behavior:

$$\sigma(T) \propto \exp(-E_a/k_B T), \quad (12)$$

with an activation energy $E_a = 0.197 \pm 0.008$ eV. This value, being actually "an weighted-mean activation energy" of the deep, E_{deep} , and the shallow, E_{sh} , states of the In ions, takes into account both the electron transfers from the deep and the shallow levels into the conduction band, and the process of transferring electrons between the deep and the shallow metastable donor levels. As can be seen from Fig. 3, at low temperatures the slope of the $\ln\sigma(1/T)$ curve decreases, corresponding to the decrease

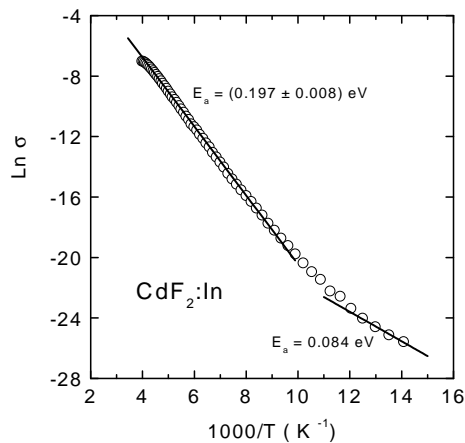


FIG. 3: Arrhenius plot of the temperature dependence of the conductivity obtained by the fitting of the experimental curves $C_p(\nu)$ and $G_p(\nu)$ for different temperatures with the Maxwell-Wagner model, Eqns. 3 and 4.

in the electron replenishment of shallow levels from the deep ones. The value of E_a , consequently, should approach the activation energy of the shallow state at quite low temperatures. This behavior has been indeed observed in Ref. [15] at temperatures 40 K to 80 K.

Since the electron mobility μ in CdF_2 depends only weakly on temperature (at the temperatures $70 \div 300$ K, $\mu \approx 15 \text{ cm}^2\text{V}^{-1}\text{s}^{-1}$ [16]), we can calculate the electron concentration n_e in the conduction band. For example, for $T = 150$ K one finds $n_e = \sigma/e\mu = 1 \cdot 10^{12} \text{ cm}^{-3}$. For this value of the electron concentration the total effective concentration of the In ions with the activation energy of $E_a = 0.197$ eV, should be $N = n_e \cdot \exp(E_a/k_B T) = 4 \cdot 10^{18} \text{ cm}^{-3}$, that coincides with $N = (3.5 \pm 0.7) \cdot 10^{18} \text{ cm}^{-3}$ obtained from our absorption coefficient data $\alpha \cong 50 \text{ cm}^{-1}$ at room temperature for $\lambda = 488$ nm.

Fig. 4 compares our results on the low-frequency conductivity in $\text{CdF}_2:\text{In}$ with the measurements in the submillimeter range carried out on a different In-doped sample at 10 K and 300 K [2] and with room-temperature infrared measurements in undoped CdF_2 [1]. The radio-frequency experimental data shown in Fig. 4, extended up to 1 GHz, were obtained on the same sample as the results of Fig. 2, but with contacts made from silver paint. The dielectric-loss results up to 1 MHz (not shown) are similar to those shown in Fig. 2. In the conductivity representation of Fig. 4, the loss peaks are transformed into a steep increase of $\sigma(\omega)$, followed by the approach of a nearly frequency-independent plateau value. The initial increase of $\sigma(\omega)$ can be ascribed to the successive shorting of the high resistance of the depletion layer by its capacitance. One should be aware that in the contact-dominated region $\sigma(\omega)$ shown in Fig. 4, which was calculated from the conductance $G(\omega)$ using the geometry of the sample, does not reflect the true conductivity of the sample material. Only when the plateau region is

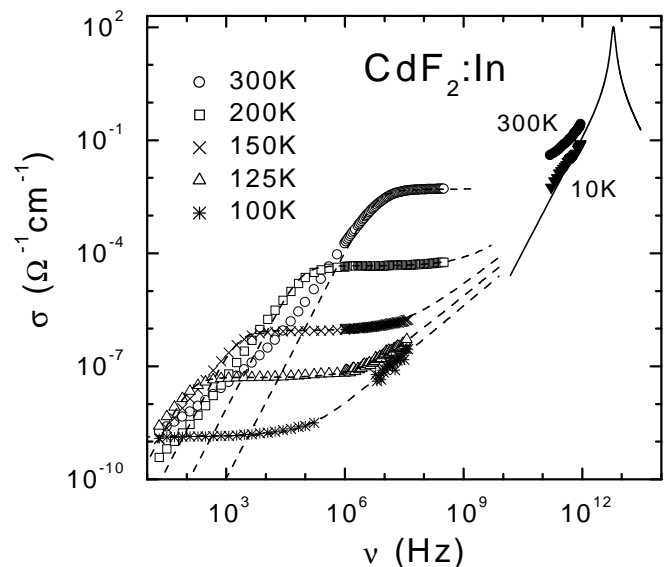


FIG. 4: Panorama spectra of the conductivity of $\text{CdF}_2:\text{In}$ with silver-paint electrodes for various temperatures (note the log-log scale). Open symbols - audio and radio-frequency measurements, solid symbols - submillimeter wave measurements [2], solid line - infrared measurements of undoped CdF_2 [1]. Dashed lines are calculated with the equivalent circuit shown in Fig. 2 with an additional UDR element for the bulk response [19, 20].

reached, the intrinsic bulk response is measured. At the lower temperatures, following this plateau, $\sigma(\omega)$ starts to increase again with increasing frequency. Such a behavior is often observed in amorphous and doped semiconductors and usually ascribed to hopping conductivity of localized charge carriers [17]. It can be parameterized by the so-called "Universal Dielectric Response" (UDR): $\sigma = \sigma_{dc} + \sigma_0 \omega^s$, $s < 1$ [18]. The dashed lines in Fig. 4 have been calculated using the equivalent circuit of Fig. 2, with an additional UDR element (including its contribution to σ'' via the Kramers-Kronig relation [18]) connected in parallel to G and C_2 [19, 20]. In this way the general behavior of the experimental spectra can be satisfactorily reproduced. Values of s between 0.8 and 0.88 were obtained, which lies in a reasonable range for hopping conduction [17]. The deviations showing up at low frequencies, again indicate that there is a non-zero conductivity of the depletion layers. For 300 K, the low-frequency curve matches well with the submillimeter data and possibly the increase of $\sigma(\omega)$ observed in the submillimeter region can also be taken into account by the UDR. Up to now UDR behavior only rarely has been observed up to such high frequencies (e.g., [20]). However, as mentioned above, the measurements in the submillimeter range were performed on a different sample, which may have a slightly different In content and therefore Fig. 4 can only provide a qualitative comparison of the low- and high-frequency response. It may be

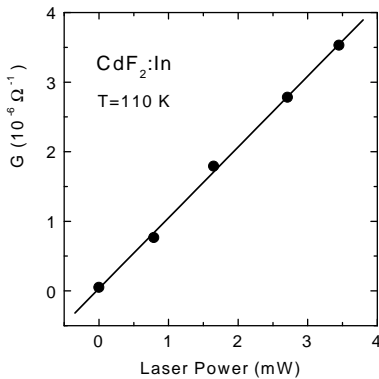


FIG. 5: The CdF₂:In sample conductance G versus the laser power at $T = 110$ K (G is obtained from the fitting of $C_p(\nu)$ and $G_p(\nu)$ curves).

noted that in CdF₂:In there is no indication for the characteristic frequency dependence connected with Drude behavior: when the frequency becomes comparable to the scattering rate of the charge carriers, a characteristic frequency-dependent decrease of the conductivity should show up. The absence of this feature possibly is due to the fact that the high-frequency conductivity seems to be governed by hopping of localized charge carriers, while Drude-like transport of "free" electrons, excited into the conduction band, dominates at low frequencies and dc only.

The submillimeter-range data for 10 K, where the low-frequency conductivity in the doped sample can be expected to be extremely low, agree well with the infrared data for CdF₂ without impurities (solid line). The latter, showing a peak at around 10^{13} Hz represents a dipolar lattice mode.

Light excitation and measurements of the shallow state kinetics

In order to determine the kinetic coefficients which affect the rate of the thermally induced transfers between the deep and shallow states, we have carried out experiments with illumination of the sample by light with a wavelength $\lambda = 488$ nm. This wavelength hits into the wide photoionization absorption band in CdF₂:In centered around 400 nm [3]. The sample was cooled to the required temperatures in darkness and illuminated afterwards. We found, that the characteristic relaxation frequency ν_p is proportional to the intensity of the light, I_{laser} , at all the temperatures (50 K \div 150 K) at which under illumination ν_p hits into the instrumental frequency window of the *HP4284* analyzer. This behavior can be ascribed to the conductivity being proportional to the light intensity (at least for that used in our experiments $I_{laser} < 6$ mW/cm²), since at $C_1 \cong const$ and $C_2 \cong const$ the conductance of the sam-

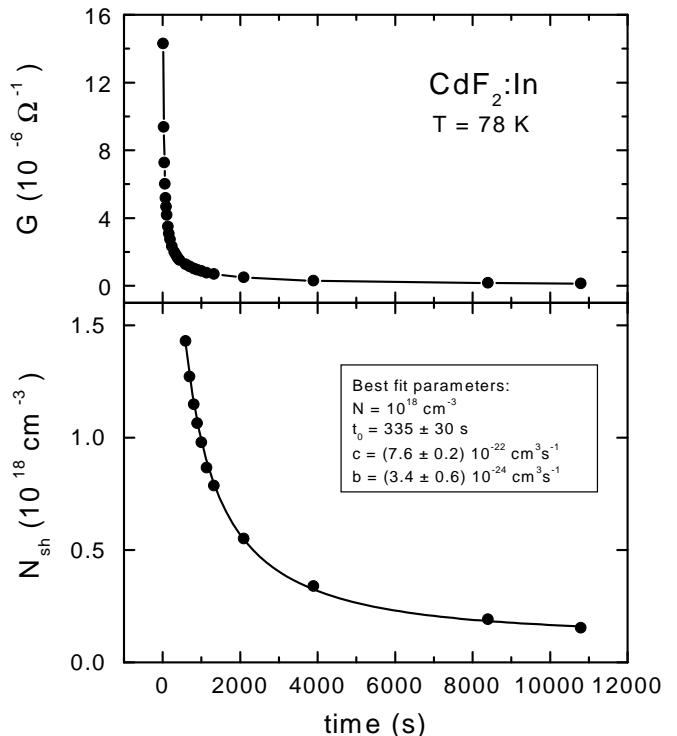
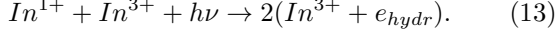


FIG. 6: Time dependencies of the conductance G (upper panel) and of the shallow donor concentration N_{sh} (bottom panel) of CdF₂:In after its irradiation with 488 nm laser light at $T = 78$ K. Upper panel: points are the experimental data, line is guided for eye. Bottom panel: points are calculated from Eqn. 20 using $n_e(t) = G(t)d/Se\mu$, and line is the best fit by Eqn. 16 (only those $G(t)$ data points have been used here, for which the calculated N_{sh} is much less than the total concentration of active impurity $N = 4 \cdot 10^{18} cm^{-3}$).

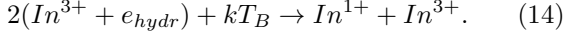
ple is $G = 2\pi\nu_p(C_1 + C_2) \propto I_{laser}$ (cf. Eqn. 11). As an example, Fig. 5 shows the sample conductance versus the laser power for $T = 110$ K. The linear dependencies $G(I_{laser})$ show the absence of any saturation effects for the illumination power used in our experiments. After switching off the illumination, the frequency ν_p and the conductance G relax with time. The rate of this relaxation is not constant. During first minutes G rapidly drops by 1 or 2 orders of magnitude, but then decreases rather gradually with a characteristic time being from half an hour to several hours (Fig. 6) depending on temperature. This process is connected with the capture of a part of the non-equilibrium carriers by the In³⁺ ions into the metastable donor state In³⁺ + e_{hydr} with a subsequent slow transition into the ground state In¹⁺. Heating the sample to room temperature and subsequent recovery cooling in darkness completely restores ν_p and the frequency dependencies of $C_p(\nu)$ and $G_p(\nu)$.

It is shown in Ref. [3], that during illumination of CdF₂:In by light with a wavelength inside of the photoionization absorption band, the following photochemi-

cal reaction takes place:



This reaction brings the In ions into the hydrogen-like state with an energy E_{sh} . The reverse process of the thermal decay of the shallow centers with capture of the released electrons by other shallow centers occurs in accordance with the bimolecular reaction:



The thermal decay of the shallow states after the light illumination is described by the kinetic equation [3]:

$$dN_{sh}/dt = -cN_{sh}^2 + b(N - N_{sh})^2/4, \quad (15)$$

where N_{sh} is the concentration of the shallow centers, c and b are the kinetic coefficients of the decay and the creation of the shallow center, correspondingly. It is assumed here, that the concentration N^{1+} of the deep centers is approximately equal to the concentration N^{3+} of the completely ionized In^{3+} centers, $N^{1+} + N^{3+} + N_{sh} = N$ and, consequently, $N^{1+} \approx N^{3+} \approx (N - N_{sh})/2$ and the free electron concentration is negligible. The solution of the Eqn. 15 yields the following time dependence for N_{sh} :

$$N_{sh}(t) = \frac{n_1 \exp \left[N\sqrt{cb}(t + t_0) \right] - n_2}{\exp \left[N\sqrt{cb}(t + t_0) \right] - 1}, \quad (16)$$

$n_1 = N/(1 + 2\sqrt{c/b})$, $n_2 = N/(1 - 2\sqrt{c/b})$, t_0 is a constant of integration.

In order to compare our results for $G(t)$ with Eqn. 16 we have calculated the electron concentration $n_e(t) = G(t)d/(Se\mu)$, and then obtained $N_{sh}(n_e)$, using the procedure described below.

Since in the $\text{CdF}_2:\text{In}$ crystals, after the additive collocation process, the In^{3+} ions play a role of donors, and the In^{1+} ions, capturing an additional electron, play a role of acceptors, and since the effective concentration of donors n_d in a compensated donor semiconductor is equal to the difference between the concentrations of donors and acceptors [21], we obtain n_d equal to the concentration of the shallow hydrogen-like centers N_{sh} , formed via capture of electrons to a hydrogen-like orbit by a little part of the In^{3+} ions. We assumed thermal equilibrium between the conduction electrons and the shallow states. We also assume that all the conduction electrons are formed through ionization of the shallow states and that the direct electron transitions between the deep levels and the conduction band are negligible. The conducting electron concentration in a semiconductor with donor and acceptor impurities with concentrations of N_d and N_a , correspondingly, is [21]:

$$N_e = \frac{N_d - N_a}{2N_a} \exp(-E_d/k_B T), \quad (17)$$

where E_d is the energy of the donor level, $N_c = 2(2\pi m^* k_B T)^{3/2}/h^3$ is the density of states in the conduction band and m^* the effective electron mass. Eqn. 17 is valid for low enough temperatures, when

$$E_d/k_B T \gg 1. \quad (18)$$

In our case $N_d \equiv N^{3+}$, $N_a \equiv N^{1+}$ and $N_d - N_a = N_{sh}$, $N^{3+} \approx N^{1+} \approx N/2$, $E_d \equiv E_{sh} = 0.1$ eV and the condition of Eqn. 18 is always satisfied. Consequently, the electron concentration is given by:

$$n_e = \frac{N_{sh}}{N} N_c \exp(-E_{sh}/k_B T), \quad (19)$$

and

$$N_{sh}(t) = (n_e(t)N/N_c) \exp(E_{sh}/k_B T). \quad (20)$$

Substituting to Eqn. 20 the data for N and $n_e(T)$, defined in our experiments ($N = 4 \cdot 10^{18} \text{ cm}^{-3}$, $n_e(T) = \sigma(T)/e\mu$), and the values of $m^* = 0.45m_e$ [16] and $E_{sh} = 0.1$ eV, we obtain $N_{sh}/n_e = 1.15 \cdot 10^7$ at $T = 78$ K and $N_{sh}/n_e = 9.07 \cdot 10^4$ at $T = 110$ K. In accordance with assumed thermal equilibrium between the conduction electrons and the shallow states we use these ratios for calculating $N_{sh}(t)$ through the experimentally found time-dependent electron density $n_e(t) = G(t)d/Se\mu$. The strong identity of the time dependencies of the infrared absorption ($\propto N_{sh}(t)$) and of the conductivity ($\propto n_e(t)$) after an optical excitation has been experimentally shown in [15]. Since Eqn. 15 implies that $N_{sh} \ll N$, we used only those experimental $G(t)$ data points, for which the calculated N_{sh} is much less than $4 \cdot 10^{18} \text{ cm}^{-3}$.

The results for $N_{sh}(t)$ and the calculated fit curve Eqn. 16 are shown in Fig. 6 (bottom part) for $T = 78$ with the best fit parameters ($N = 10^{18} \text{ cm}^{-3}$, $t_0 = 335$ s, $c = 7.6 \cdot 10^{-22} \text{ cm}^3 \text{ s}^{-1}$, and $b = 3.4 \cdot 10^{-24} \text{ cm}^3 \text{ s}^{-1}$). For the thermal decay curve at $T = 110$ K the best fit parameters are $N = 4 \cdot 10^{18} \text{ cm}^{-3}$, $t_0 = 2875$ s, $c = 1.17 \cdot 10^{-19} \text{ cm}^3 \text{ s}^{-1}$, and $b = 3.7 \cdot 10^{-25} \text{ cm}^3 \text{ s}^{-1}$. Using these values of c and b , we compare the shallow center decay and creation processes for $T = 78$ K and $T = 110$ K. At $t = 1000$ s and $T = 78$ K, the first term of Eqn. 15 is two orders of magnitude larger than the second one, i.e. the thermal decay of the shallow states is dominating. At $T = 110$ K and $t = 1000$ s these terms are nearly equal, i.e. the thermal decay begins to be compensated by the thermal activation. It is interesting, that $c(110 \text{ K})$ is two orders of magnitude larger than $c(78 \text{ K})$, while $b(110 \text{ K})$ is one order of magnitude smaller than $b(78 \text{ K})$.

Assuming that the temperature dependence of the kinetic coefficient c can be described by activated behavior, $c(T) = A \cdot \exp(-E_{ac}/k_B T)$, from $c(78 \text{ K})$ and $c(110 \text{ K})$ we found $E_{ac} = 0.12$ eV. This value coincides with E_{ac} obtained in [3] by the kinetic measurements of the shallow state infrared absorption. The kinetic coefficient c may be presented as $c(T) = \text{const} \cdot p_1 \cdot p_2$, where

$p_1 = \nu_1 \cdot \exp(-E_{sh}/k_B T)$ is the rate of the electron releasing out the first shallow center to the conduction band, and $p_2 = \nu_2 \cdot \exp(-E_{cap}/k_B T)$ is the rate of the thermally activated electron hopping over the barrier E_{cap} and simultaneous capture of a conduction electron by the second shallow center [3]. Here ν_1 and ν_2 are the attempt frequencies: ν_1 is the impurity vibration frequency and ν_2 is the "configuration phonon mode" frequency of the impurity. The electron-impurity collision frequency ν_{coll} in our case is much higher than ν_2 : since the electron mobility at $T \leq 150$ K is determined mainly by the ionized impurity scattering [16], the first can be calculated as $\nu_{coll} \approx e/m^* \mu = 2.6 \cdot 10^{14}$ Hz, while for the last the upper estimate would be the Debye frequency $\nu_{Debye} \approx 6 \cdot 10^{12}$ Hz. Thus, at least several dozens of electron-impurity collisions occur during one cycle of the impurity "configuration phonon mode" and at the moment of the local lattice distortion near the In impurity there is always a conduction electron ready to be captured. Thus, for the activation energy of the kinetic coefficient c one has $E_{ac} = E_{sh} + E_{cap}$, and the capture barrier is equal to $E_{cap} = E_{ac} - E_{sh} = 0.12$ eV - 0.1 eV = 0.02 eV.

For a higher temperature ($T = 150$ K) the shallow state decay curve is not fitted exactly by Eqn. 16. The change of the decay kinetics type on increasing temperature may be explained by formation of a shallow states impurity band in $\text{CdF}_2:\text{In}$. The levels of the hydrogen-like states $\text{In}^{3+} + e_{hydr}$ may form such a band due to Coulomb interaction with statistically distributed F^{1-} , In^{3+} and In^{1+} ions [15]. For increasing temperature, the higher levels of this band become populated, leading to an effective decrease of E_{cap} . At $T = 150$ K the levels up to $k_B T = 0.013$ eV $\approx E_{cap}$ are populated and the barrier is eliminated.

The knowledge of the key parameters $E_{cap} = 0.02$ eV, $E_{sh} = 0.1$ eV [8], $E_{deep} = 0.25$ eV [5, 8], $E_{opt} = 1.9$ eV [5] (the optical ionization energy of the deep state) and $Q_0 - Q_1 = 1.84$ Å [8] (the difference of configuration coordinates of the deep and the shallow states) allows to define concretely the energy diagram (presented schematically in Fig. 1), assuming $Q_1 = 0$ and a quadratic Q -dependence of the levels:

$$\begin{aligned} E_{cond}(Q) &= a_1 Q^2, \\ E_{sh}(Q) &= a_1 Q^2 - E_{sh}, \\ E_{deep}(Q) &= a_0 (Q - Q_0)^2 - E_{deep}. \end{aligned} \quad (21)$$

Here the energies are measured in eV and the coordinates are in Angstroms. Then for a_1 and a_0 one has:

$$\begin{aligned} a_1 &= \frac{E_{opt} - E_{deep}}{Q_0^2}, \\ a_0 &= \frac{E_{deep} - E_{sh} + E_{cap}}{(Q_{cap} - Q_0)^2}, \\ Q_{cap} &= \sqrt{\frac{E_{cap}}{a_1}}, \end{aligned} \quad (22)$$

consequently, $a_1 = 0.487$ eV/Å², $a_0 = 0.063$ eV/Å², $Q_{cap} = 0.20$ Å. The corresponding diagram is given in

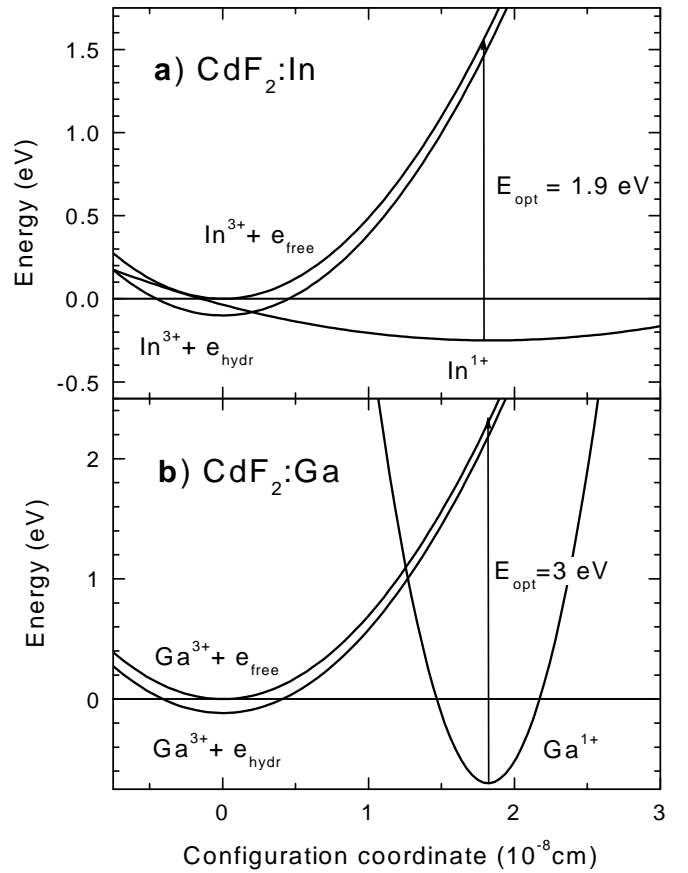


FIG. 7: Specified energy levels diagrams for the deep and the shallow states of the bistable In (a) and Ga (b) center in CdF_2 , as function of the configuration coordinate Q of the impurity ion nucleus.

Fig. 7a, which shows that the walls of the potential well of the shallow states are much steeper than those of the deep state. Therefore, according to the values of a_1 and a_0 , the "return force" $F = -dE/dQ$ is 8 times larger for the shallow state. Besides, the barrier position Q_{cap} is very close to the potential well minimum of the shallow state. It is interesting to note, that a similar calculation made for CdF_2 doped with Ga ($E_{sh} = 0.116$ eV [22], $E_{opt} = 3$ eV, $E_{cap} = 1.12$ eV [23], $E_{deep} = 0.7$ eV and $Q_0 - Q_1 = 1.82$ Å [5]) gives the opposite picture of the potential curves (Fig. 7b). Now $a_1 = 0.694$ eV/Å², $a_0 = 5.63$ eV/Å², $Q_{cap} = 1.27$ Å, i.e. the "return force" for the shallow state is 8 times weaker than one for the deep state, and the barrier position Q_{cap} is far away from the shallow state potential well minimum. In addition, while the "return forces" for the shallow states of In and Ga in CdF_2 are close to each other, the "return force" for the deep state of Ga is 90 times larger than one for In. Now we can calculate the impurity "configuration phonon mode" frequencies of the deep, $\nu_{deep} = \frac{1}{2\pi} \sqrt{2a_0/M}$, and of the shallow, $\nu_{sh} = \frac{1}{2\pi} \sqrt{2a_1/M}$, states. Here M is the

reduced mass of the impurity ion and of the surrounding ions, involved in the "configuration phonon modes". As the first approximation we have taken the values of the impurity ions masses for M and obtained for the In impurity $\nu_{deep} = 5.18 \cdot 10^{11}$ Hz, $\nu_{sh} = 1.44 \cdot 10^{12}$ Hz and for the Ga impurity $\nu_{deep} = 6.28 \cdot 10^{12}$ Hz, $\nu_{sh} = 2.2 \cdot 10^{12}$ Hz.

We should note, that the data obtained for the values of kinetic coefficients are at some extent qualitative, because the assumption that the direct transitions between the deep levels and the conduction band is negligible is not strongly fulfilled in CdF₂:In at temperatures between 78 and 150 K. Nevertheless, the used ratios N_{sh}/n_e calculated by the simple approximate Eqn. 20 for $T = 78$ K and $T = 110$ K coincided within a few tenth of a percent with the ratios obtained with the formulae of exact statistical calculation derived in [11]. Similar measurements and data analysis for the CdF₂:Ga crystals would give accurate results, since in this crystal $E_{deep} = 0.7$ eV [5], and the assumption mentioned above is fulfilled. Unfortunately, the CdF₂:Ga samples reveal often some amount of the In impurities as well [24], influencing the experimental results, since there are actually two activation energies and two capture barriers in these samples.

CONCLUSIONS

In this paper we report on the low frequency conductivity measurements of semiconducting CdF₂:In crystals with metal-coating electrodes, producing Schottky barriers at the sample surface. The results allow to determine a whole lot of the material characteristics: the temperature dependence of the dc conductivity, the activation energy of the impurity E_a , the total concentration of the active In ions N , the shallow donor concentration N_{sh} , the height of the capture barrier E_{cap} , and the values of the kinetic coefficients determining the rate of the thermally induced transitions between the deep and shallow states of In in the CdF₂ matrix. These measurements do not require ohmic contacts, preparation of which is necessary for standard dc measurements and often is quite complicated and not always realizable task.

ACKNOWLEDGEMENTS

The work was supported by BMBF (contract 13N6917/0 - EKM), CRDF (project RP1-2096) and RFBR (project 99-02-16859).

- [2] A.V. Pronin et al., unpublished.
- [3] A.S. Shcheulin, A.I. Ryskin, K. Swiatek, J.M. Langer, Phys. Lett. A **222**, 107 (1996).
- [4] S.A. Kazanskii, A.I. Ryskin, V.V. Romanov, Appl. Phys. Lett. **70**, 1272 (1997); Phys. Solid State **39**, 1067 (1997).
- [5] C.H. Park, D.J. Chadi, Phys. Rev. Lett. **82**, 113 (1999).
- [6] D.J. Chadi, K.J. Chang, Phys. Rev. Lett. **61**, 873 (1988).
- [7] Tineke Thio, J.W. Bennett, P. Becla, Phys. Rev. B **54**, 1754 (1996).
- [8] J.M.Langer, Lecture Notes in Physics **122**, 123 (1980).
- [9] A.I. Ryskin, A.S. Shcheulin, B. Koziarska, J.M. Langer, A. Suchocki, I.I. Buchinskaya, P.P. Fedorov, B.P. Sobolev, Appl. Phys. Lett. **67**, 31 (1995).
- [10] A. Suchocki, B. Koziarska, T. Langer, and J.M. Langer, Appl. Phys. Lett. **70**, 2934 (1997).
- [11] A.S. Shcheulin, A.K. Kupchikov, A.E. Angervaks, D.E. Onopko, A.I. Ryskin, A.I. Ritus, A.V. Pronin, A.A. Volkov, P. Lunkenheimer, and A. Loidl, Phys. Rev. B **63**, 205207 (2001).
- [12] R. Böhmer, M. Maglione, P. Lunkenheimer, and A. Loidl, J. Appl. Phys. **65**, 901 (1989).
- [13] A. Hippel, *Dielectrics and waves* (John Wiley and Sons, Inc., NY, Chapman and Hall Limited, London) 1954.
- [14] Ch. Kittel, *Introduction to Solid State Physics*, (John Wiley and Sons, Inc., NY-London) 1956.
- [15] I. Kunze and W. Ulrici, Phys. Stat. Solidi (b) **55**, 567 (1973).
- [16] R.P. Khosla and D. Matz, Solid State Commun. **6**, 859 (1968); R.P. Khosla, Phys. Rev. **183**, 695 (1969).
- [17] S.R. Elliott, Adv. Phys. **36**, 135 (1987); A.R. Long, Adv. Phys. **31**, 553 (1982).
- [18] A.K. Jonscher, *Dielectric Relaxation in Solids* (Chelsea Dielectrics Press, London) 1983.
- [19] P. Lunkenheimer, M. Resch, A. Loidl, and Y. Hidaka, Phys. Rev. Lett. **69**, 498 (1992); A. Seeger, P. Lunkenheimer, J. Hemberger, A.A. Mukhin, V.Yu. Ivanov, A.M. Balbashov, and A. Loidl, J. Phys.: Cond. Matter **11**, 3273 (1999).
- [20] J. Sichelschmidt, M. Paraskevopoulos, M. Brando, R. Wehn, D. Ivannikov, F. Mayr, K. Pucher, J. Hemberger, A. Pimenov, H.-A. Krug von Nidda, P. Lunkenheimer, V.Yu. Ivanov, A.A. Mukhin, A.M. Balbashov, and A. Loidl, Euro. Phys. J. B **20**, 7 (2001).
- [21] R.A. Smith, *Semiconductors* (Cambridge University Press, London - New York - Melbourne) 1978.
- [22] J.M. Langer, T. Langer, G.L. Pearson, B. Krukowska-Fulde, and U. Piekara, Phys. Stat. Solidi (b) **66**, 537 (1974).
- [23] A.I. Ryskin, A.S. Shcheulin, D.E. Onopko, Phys. Rev. Lett. **80**, 2949 (1998).
- [24] B. Koziarska-Glinka, A. Barcz, L. Arizmendi, A. Suchocki, Phys. Rev. B **61**, 9295 (2000).

[1] J.D. Axe, J.W. Gaglianella, and J. E. Scardefield, Phys. Rev. **139**, A1211 (1965).